Available online at www.sciencedirect.com
ScienceDirect
Comput. Methods Appl. Mech. Engrg. 196 (2007) 4479–4494
Computer methods in applied mechanics and engineering
www.elsevier.com/locate/cma

A divergence-free-condition compensated method for incompressible Navier–Stokes equations

Tony W.H. Sheu *, P.H. Chiu

Department of Engineering Science and Ocean Engineering, National Taiwan University, No. 1, Sec. 4, Roosevelt Road, Taipei 106, Taiwan, ROC

Received 13 March 2007; received in revised form 4 May 2007; accepted 14 May 2007
Available online 7 June 2007

Abstract

The present study aims to develop a new formulation to effectively calculate the incompressible Navier–Stokes solutions in non-staggered grids. The distinguished feature of the proposed method, which avoids directly solving the divergence-free equation, is to add a rigorously derived source term to the momentum equation to ensure satisfaction of the fluid incompressibility. For the sake of numerical accuracy, dispersion-relation-preserving upwind scheme developed within the two-dimensional context was employed to approximate the convection terms. The validity of the proposed mass-preserving Navier–Stokes method is justified by solving two benchmark problems at high Reynolds and Rayleigh numbers. Based on the simulated Navier–Stokes solutions, the proposed formulation is shown to outperform the conventional segregated method in terms of the reduction of CPU time.

Keywords: Incompressible; Navier–Stokes equations; Non-staggered grids; Rigorously derived source term; Dispersion-relation-preserving

1. Introduction

For more than five decades, numerical prediction of practically important viscous incompressible fluid flows has been the focus of the CFD community after the pioneering works of Fromm and Harlow [1] and Harlow and Welch [2]. This differential system for the fluid flow has gained importance because the predicted solution is susceptible to various types of numerical oscillation. One well-known oscillation arises from the central approximation of convection terms shown in this class of differential equations. To eliminate the oscillations, which primarily occur in the velocity field, one can approximate the convective terms by means of upwinding schemes [3]. However, upwinding approximation of convective terms can give rise to false diffusion error as the spatial dimension exceeds one [4]. Therefore, the chosen flux discretization scheme should dispense with the cross-wind diffusion error without sacrificing the convective stability. Another type of numerical oscillation frequently encountered in the analysis of incompressible flow equations, cast in primitive variables, is due to the predicted oscillatory pressure values manifested by the checkerboard pattern. On the non-staggered (collocated) grids, numerical oscillation is evident if a conventional central differencing scheme is used to approximate the pressure gradient term in the momentum equations and the cell-face velocity in the approximation of continuity equation [5]. The oscillatory solution is featured with two separate pressure solutions at the alternating nodes owing to the decoupling of velocity and pressure fields. For these reasons, many studies have been motivated to resolve the checkerboard problem without resorting to the staggered grid approaches. The need to suppress oscillations of velocity and pressure origins without accuracy deterioration has motivated our previous study [6].

Another computational challenge encountered in the calculation of incompressible viscous flow equations is due to the velocity field which should be always divergence-free. The incompressibility constraint condition $\nabla \cdot \underline{u} = 0$ required for coupling $\underline{u}$ and p limits the arbitrary choice of functional spaces for the velocity and pressure. In

* Corresponding author. Tel.: +886 2 33665791; fax: +886 2 23929885.
E-mail address: twhsheu@ntu.edu.tw (T.W.H. Sheu).

0045-7825/$ - see front matter © 2007 Elsevier B.V. All rights reserved.
doi:10.1016/j.cma.2007.05.015

fact, this set of primitive variables should satisfy the Babuska–Brezzi inf–sup condition [7]. To conserve the mass, the mixed formulation, which solves the equations of motion in conjunction with the incompressible constraint condition, is employed. It is, however, obvious that calculation of the velocity–pressure coupled discrete equations is quite expensive. Moreover, the resulting large-sized matrix equations become diagonally weak and may accommodate poor eigenvalue distribution. These drawbacks make the calculation of primitive variables from the incompressible Navier–Stokes equations an even challenging issue.

The necessity of resolving the divergence-free constraint condition and the convective instability problems inherent in the velocity–pressure mixed formulation for the incompressible Navier–Stokes equations has motivated the development of projection approach [8,9]. This class of methods, which are featured with the decomposition of the L^2 – vector fields into the sum of divergence-free and curl-free fields [10], can be interpreted as the splitting algorithms in time. Within the framework of fractional-step methods, over each time step the solution will be updated through two or more stages. In the first temporal stage, momentum equations are normally solved for an approximated velocity vector, which is not necessarily to be divergence-free. The intermediate velocity vector is then projected into the divergence-free space by means of a Poisson equation, which can be cast in different forms, for the updated pressure. The difficulties of simultaneously coping with divergence-free condition and suppressing the convective instability are revolved.

Besides the projection and pressure–Poisson formulations, the pseudo-compressibility and penalty methods, which can regularize the primitive-variable Navier–Stokes equations, have been shown to be able to enhance numerical stability and reduce computational cost. The underlying idea of the pseudo-compressibility methods is to replace the incompressibility constraint condition with, for example, the following three equations: (i) $\nabla \cdot \underline{u} + \epsilon p = 0$; (ii) $\nabla \cdot \underline{u} + \epsilon \frac{\partial p}{\partial t} = 0$ and (iii) $\nabla \cdot \underline{u} - \epsilon \nabla^2 p = 0$, where $\frac{\partial p}{\partial n}|_{\partial D} = 0$ on the boundary ∂D. The prescribed perturbation parameter ϵ, which will be addressed in Sections 3.1 and 5.2, plays an essential role to determine the computational effectiveness. Application of penalty method is another effective way for the calculation of velocity and pressure solutions separately. Moreover, this method has the benefit of not necessarily invoking the pressure–Poisson equation. The explicit transient MAC method [2] and the implicitly updating SIMPLE method [4] are known to be the two representative primitive-variable methods for solving the incompressible flow equations. A more recently proposed gauge method [11] was also developed to replace the pressure variable with the gauge variable Φ by introducing an auxiliary vector field $\underline{a}$, which differs from the velocity $\underline{u}$ by an amount of $\nabla\Phi$. The advantage of employing this formulation is that the boundary conditions for $\underline{a}$ and Φ can be unambiguously assigned, thus eliminating the problem of pressure boundary value. Recently, the sequential regularization method (SRM) proposed by Bayo and Avello [12] for the constrained mechanical system drew much interest in solving the time-dependent incompressible Navier–Stokes equations [14,13]. One prevailing advantage of employing the SRM is that a fully explicit scheme can be used to calculate the truly transient solution. No need is required to solve the linear system of momentum equations and pressure correction equation. Specification of pressure boundary values can thus be avoided.

This paper is organized as follows. Section 2 presents the primitive-variable Navier–Stokes equations. This is followed by presenting the proposed divergence-free-condition (DFC) compensated method. Section 4 describes the methods for appropriately decoupling the velocity–pressure field in non-staggered grids and the two-dimensional dispersion-relation-preserving (DRP) scheme for the approximation of the first-order derivative terms. Both dispersion and Fourier (or von Neumann) stability analyses will be carried out for the employed convection–diffusion–reaction (CDR) discretization scheme. Section 5 presents the simulated results to validate the DRP convection scheme. In Section 6, some concluding remarks are given.

2. Governing equations

In this study the viscous incompressible flow equations, including the continuity and momentum equations cast in the primitive-variable pair $(\underline{u}, p)$, are solved at the Reynolds number Re:

$$\nabla \cdot \underline{u} = 0, \tag{2.1}$$

$$\frac{\partial \underline{u}}{\partial t} + (\underline{u} \cdot \nabla)\underline{u} - \frac{1}{Re}\nabla^2 \underline{u} + \nabla p = \underline{f}. \tag{2.2}$$

In the above, $\underline{f}$ represents the source term. Given the initial divergence-free velocity field and the boundary velocity, the chosen primitive variables $\underline{u}$ and p will be sought in a region Ω with the boundary $\partial\Omega$. The condition applied at $\partial\Omega$ with an outward normal vector $\underline{n}$ must satisfy $\oint_{\partial\Omega} \underline{u} \cdot \underline{n}\, ds = 0$.

Subjected to the constraint Eq. (2.1), the differential system governing the viscous flow motion is not entirely evolutionary. Momentum equations can be solved along with the divergence-free Eq. (2.1). Unconditional satisfaction of the constraint condition for preserving the mass conservation (or incompressibility) can, however, result in a matrix system which is not normally well-conditioned. Under the circumstance, the convergent solutions for $(\underline{u}, p)$ become more difficult to be obtained using a computationally less expensive iterative solver [15]. In certain cases, the peripheral storage for the matrix equations may exceed the available computer power and disk space. These drawbacks led to the derivation of a scalar equation for p to replace Eq. (2.1). This class of approaches is subjected to the rigorously derived integral condition for the pressure [16] and is, therefore, computationally more challenging to be dealt with. Due to the above drawbacks in the computation of time-dependent incompressible

Navier–Stokes equations, Lin [14] proposed the sequential regularization method without invoking any specification of pressure boundary value. In the present study, a computationally effective and novel method will be developed in Section 3 for the time-dependent Navier–Stokes equations.

3. Divergence-free-condition compensated method

3.1. Some underlying theories

Development of regularized methods for solving the computationally difficult Navier–Stokes equations along with the incompressibility constraint condition is rooted in replacing the divergence-free constraint equation for mass conservation with a differential equation for pressure or pressure variation. The fractional step and artificial compressibility methods are the two representative classes and will be briefly reviewed below. In the artificial compressibility method, the constraint equation for the velocity field, which is governed by Eq. (2.2), is regularized by adding a pseudo-time-dependent term $\frac{1}{\beta}\frac{\partial p}{\partial \tau}$ to the left-hand-side of Eq. (2.1). The equation representing mass conservation turns out to be the following equation for p:

$$\frac{1}{\beta}\frac{\partial p}{\partial \tau} + \nabla \cdot \underline{u} = 0. \tag{3.1}$$

While it is very sensitive to obtain the convergent solution from Eqs. (2.2) and (3.1) due to the user's specified artificial compressibility coefficient β (10–500 was recommended in [17,18]), Eq. (3.1) is served to be the guidance to update the pressure value by an amount of $\beta\nabla \cdot \underline{u}$ between the two pseudo-times (or iterations).

Another approach to approximate Eqs. (2.1) and (2.2) is to employ the fractional-step methods. In this semi-discrete formulation, approximation of equations can be generally decomposed into two or three steps. The first step, which approximates the viscous and convective terms, consists of finding an intermediate velocity from the transport equation for $\underline{u}$ with the pressure term being omitted. This step can, thus, be considered as a linearized viscous Burgers' problem. To make the fractional-step method viable for solving the incompressible Eqs. (2.1) and (2.2), the time advancement should be accurately split. Thanks to the Helmholtz–Hodge decomposition theorem [19], which enables us to decompose any vector field $\underline{w}$ into a solenoidal field with the zero normal component on the boundary and the gradient of some scalar functions. By choosing the scalar function as Φ and the divergence-free vector field as the velocity $\underline{u}$, the following equation is resulted from the Helmholtz–Hodge decomposition theorem

$$\underline{u} = \underline{w} - \nabla\Phi. \tag{3.2}$$

Define an operator P such that $P(\underline{w}) = \underline{u}$. In other words, use of this operator can project any vector field $\underline{w}$ to its divergence-free part, namely, $\underline{u}$. Application of operator P on Eq. (3.2) can render $P(\underline{w})$ as $P(\underline{u}) + P(\nabla\Phi)$ and, in turn, $P(\nabla\Phi) = 0$ by virtue of the definition of P (or $P(\underline{w}) = \underline{u}$). The operator P is then applied to both hand sides of Eq. (2.2), for example, to render

$$P\frac{\partial \underline{u}}{\partial t} = P\left(-(\underline{u}\cdot\nabla)\underline{u} - \nabla p + \frac{1}{Re}\nabla^2\underline{u} + \underline{f}\right). \tag{3.3}$$

Since $\underline{u}$ is divergence-free, the derivative term on the left-hand-side of the above equation is also divergence-free, thereby yielding $P(\frac{\partial \underline{u}}{\partial t}) = \frac{\partial \underline{u}}{\partial t}$. Eq. (3.3) can be therefore reduced to

$$\frac{\partial \underline{u}}{\partial t} = P\left(-(\underline{u}\cdot\nabla)\underline{u} - \nabla p + \frac{1}{Re}\nabla^2\underline{u} + \underline{f}\right). \tag{3.4}$$

Use of the above employed orthogonal splitting operator can decouple the convective term from the constrained incompressibility condition, which is known to be the major difficulty in the simulation of viscous incompressible flow equations. Thanks to this theoretically splitting equation, the vector field can be decomposed into the zero-curl and zero-divergence parts. The intermediate velocity $\underline{u}^{n+\frac{1}{2}}$ can then be calculated from the fully implicit equation along with the prescribed boundary velocity $\underline{u}^{n+\frac{1}{2}}|_{\partial\Omega} = \underline{b}$ as

$$\frac{\underline{u}^{n+\frac{1}{2}} - \underline{u}^{n}}{\Delta t} = -(\underline{u}^{n+\frac{1}{2}}\cdot\nabla)\underline{u}^{n+\frac{1}{2}} + \frac{1}{Re}\nabla^2\underline{u}^{n+\frac{1}{2}} + \underline{f}^{n+\frac{1}{2}}. \tag{3.5}$$

Note that the pressure variable has been eliminated from the momentum equations. Analysis of incompressible viscous equations becomes therefore much simplified. For the value of $\underline{u}^{n+\frac{1}{2}}$, it can be also calculated sequentially from the advection and diffusion steps based on the Marchuk–Yanenko fractional-step method [20]. Use of this method can separate the convective term from the viscous diffusion term. The advection step, given by $\frac{\underline{u}_a^{n+\frac{1}{2}} - \underline{u}^n}{\Delta t} + (\underline{u}^n\cdot\nabla)\underline{u}^n = 0$, and the diffusion step, given by $\frac{\underline{u}^{n+\frac{1}{2}} - \underline{u}_a^{n+\frac{1}{2}}}{\Delta t} = \frac{1}{Re}\nabla^2\underline{u}^{n+\frac{1}{2}} + \underline{f}^{n+\frac{1}{2}}$, are resulted. Note that the intermediate velocity solution $\underline{u}^{n+\frac{1}{2}}$ obtained from the above two steps does not satisfy the divergence-free constraint condition. Then the intermediate field $\underline{u}^{n+\frac{1}{2}}$ (or $\underline{w}$ given in Eq. (3.2)) is decomposed into the sum of the solenoidal velocity field $\underline{u}^{n+1}$ and the gradient of the currently chosen scalar function, which is proportional to $\Delta t\nabla p^{n+1}$. This enlightens the integrity of employing the following two equations in the projection step

$$\frac{\underline{u}^{n+1} - \underline{u}^{n+\frac{1}{2}}}{\Delta t} = -\nabla p^{n+1}, \tag{3.6}$$

$$\nabla \cdot \underline{u}^{n+1} = 0. \tag{3.7}$$

As the Eq. (3.6) implies, calculation of $\underline{u}^{n+1}$ needs a pressure solution. By applying the divergence operator to both hand sides of Eq. (3.2), the following Poisson equation for the pressure is derived by virtue of Eq. (3.7)

$$\nabla^2 p = \nabla \cdot \underline{u}^{n+\frac{1}{2}}. \tag{3.8}$$

The above equation can be considered as the incompressibility condition. Controversy arises regarding the necessity of specifying the pressure boundary value for Eq. (3.8)

since no pressure boundary value is needed to be specified when solving Eqs. (2.1) and (2.2). The resulting incompatibility of the projection boundary conditions with those for the continuous problem defined by Eqs. (2.1) and (2.2) may cause a numerical boundary layer of width $O((\nu\Delta t)^{\frac{1}{2}})$ to develop [21,22]. Besides the numerically generated boundary layer artifact, analysis of the Poisson equation for p is also computationally expensive. For these reasons, in the following section the regularization method is proposed.

3.2. Divergence-free-condition compensated method

Development of the proposed regularization method begins with the substitution of Eq. (3.6) into the following semi-discretized momentum equation for (2.2)

$$\frac{\underline{u}^{n+1}-\underline{u}^{n}}{\Delta t}+(\underline{u}^{n+1}\cdot\nabla)\underline{u}^{n+1}-\frac{1}{Re}\nabla^2\underline{u}^{n+1}+\nabla p^{n+1}=\underline{f}^{n+1}. \tag{3.9}$$

This substitution yields

$$\frac{\underline{u}^{n+1}-\underline{u}^{n}}{\Delta t}+(\underline{u}^{n+\frac{1}{2}}\cdot\nabla)\underline{u}^{n+\frac{1}{2}}-\frac{1}{Re}\nabla^2\underline{u}^{n+\frac{1}{2}}+\nabla p^{n+1} =\underline{f}^{n+1}+M_1+M_2, \tag{3.10}$$

where $M_1=[(\underline{u}^{n+\frac{1}{2}}\cdot\nabla)\nabla p^{n+1}+(\nabla p^{n+1}\cdot\nabla)\underline{u}^{n+\frac{1}{2}}-\frac{1}{Re}\nabla^2(\nabla p^{n+1})]\Delta t$ and $M_2=-[(\nabla p^{n+1}\cdot\nabla)\nabla p^{n+1}]\Delta t^2$. Let $p^{n+1}=p^*+p'$, where p^* can be initially chosen to be the computed convergent solution p^n. Afterwards, the value of p^* will be chosen as the most updated value. The pressure gradient step is decomposed into the following two steps

$$\frac{\underline{u}^{*}-\underline{u}^{n+\frac{1}{2}}}{\Delta t}=-\nabla p^{*}, \tag{3.11}$$

$$\frac{\underline{u}^{n+1}-\underline{u}^{*}}{\Delta t}=-\nabla p'. \tag{3.12}$$

Then Eq. (3.10) can be reformulated as

$$\frac{\underline{u}^{n+1}-\underline{u}^{n}}{\Delta t}+(\underline{u}^{*}\cdot\nabla)\underline{u}^{*}-\frac{1}{Re}\nabla^2\underline{u}^{*}+\nabla p^{*} =\underline{f}^{n+1}-\nabla p'+M_3+M_4, \tag{3.13}$$

where

$$M_3=\left[(\underline{u}^{*}\cdot\nabla)\nabla p'+(\nabla p'\cdot\nabla)\underline{u}^{*}-\frac{1}{Re}\nabla^2(\nabla p')\right]\Delta t, \tag{3.14}$$

$$M_4=-[(\nabla p'\cdot\nabla)\nabla p']\Delta t^2. \tag{3.15}$$

By taking the divergence of Eq. (3.12) and imposing the constraint condition $\nabla\cdot\underline{u}^{n+1}=0$, Eq. (3.14) can be rewritten as

$$M_3=[(\underline{u}^{*}\cdot\nabla)\nabla p'+(\nabla p'\cdot\nabla)\underline{u}^{*}]\Delta t-\frac{1}{Re}\nabla(\nabla\cdot\underline{u}^{*}). \tag{3.16}$$

We denote the right-hand-side of Eq. (3.13) as M_{DFC}. The introduced momentum source term M_{DFC} plays the role of ensuring the divergence-free condition and can be called as the divergence-free-condition (DFC) compensated momentum source term. In other words, the main concept of the proposed compensated method is to replace the divergence-free constraint condition with the momentum source term, which is added to the momentum equations. Note that the Lin's SRM [14] given below.

For $m=1,2,\ldots$

$$\frac{\partial\underline{u}_m}{\partial t}+\underline{u}_m\cdot\nabla\underline{u}_m-\frac{1}{Re}\nabla^2\underline{u}_m+\nabla p_{m-1}=\lambda\nabla(\nabla\cdot\underline{u}_m), \tag{3.17}$$

$$p_m=p_{m-1}-\lambda(\nabla\cdot\underline{u}_m) \tag{3.18}$$

falls also into the category of the DFC compensated method provided that $\underline{f}=0$, $M_{\mathrm{DFC}}=\lambda\nabla(\nabla\cdot\underline{u}_m)$ and $p'=\lambda(\nabla\cdot\underline{u}_m)$.

In the present study, the aim of developing a compensated method is to avoid dealing with the computationally challenging divergence-free constraint equation. As the divergence-free constraint condition is satisfied, the DFC momentum source will be disappeared. For the steady-state analysis, the convergent tolerance defined by $E(\equiv\max|\phi^{n+1}-\phi^n|)$, where ϕ represents the field variable for $\underline{u}$ or p, is set as $E\leqslant 10^{-6}$. For the transient case, the time-accurate solution can be iteratively obtained. After obtaining the updated values for velocity and pressure at every iteration, they are substituted into the left-hand-side of Eq. (3.10) to calculate the momentum source term. As the momentum source term becomes smaller than 10^{-4}, the solution at each time step is assumed to be convergent.

Now, the remaining issue of the proposed compensated method is to derive the equation for p'. By performing the divergence operator on Eq. (3.12), we get

$$\nabla\cdot\underline{u}^{n+1}=\nabla\cdot\underline{u}^{*}-\Delta t\nabla^2p'. \tag{3.19}$$

Enforcement of the divergence-free condition $\nabla\cdot\underline{u}^{n+1}=0$ yields

$$\nabla^2p'=\frac{\nabla\cdot\underline{u}^{*}}{\Delta t}. \tag{3.20}$$

At an interior point (i,j), central approximation of the left-hand-side of Eq. (3.20) leads to

$$2\left(\frac{1}{\Delta x^2}+\frac{1}{\Delta y^2}\right)p'_{i,j}=-\frac{\nabla\cdot\underline{u}^{*}_{i,j}}{\Delta t}+\frac{1}{\Delta x^2}(p'_{i-1,j}+p'_{i+1,j}) +\frac{1}{\Delta y^2}(p'_{i,j-1}+p'_{i,j+1}). \tag{3.21}$$

By omitting $\frac{1}{\Delta x^2}(p'_{i-1,j}+p'_{i+1,j})+\frac{1}{\Delta y^2}(p'_{i,j-1}+p'_{i,j+1})$, the following equation can be derived:

$$p'_{i,j}=-\frac{\Delta x^2\Delta y^2}{2(\Delta x^2+\Delta y^2)\Delta t}\nabla\cdot\underline{u}^{*}_{i,j}. \tag{3.22}$$

The above omission may over-estimate the predicted pressure solution p'. A compensation for the omission of two terms will be made as follows. First, Eq. (3.22) is used to obtain the following predicted pressure correction p'^{*}

$$p'^{*}_{i,j}=-\frac{\Delta x^2\Delta y^2}{2(\Delta x^2+\Delta y^2)\Delta t}\nabla\cdot\underline{u}^{*}_{i,j}. \tag{3.23}$$

This is followed by calculating the pressure correction p' from p'^* by taking into account the two omitted terms, which are evaluated using the p'^* solutions. The resulting p' solution at (i,j), for example, is calculated according to

$$p'_{i,j} = p'^*_{i,j} + \frac{\Delta y^2}{2(\Delta x^2+\Delta y^2)}(p'^*_{i-1,j}+p'^*_{i+1,j}) + \frac{\Delta x^2}{2(\Delta x^2+\Delta y^2)}(p'^*_{i,j-1}+p'^*_{i,j+1}). \tag{3.24}$$

Note that under-relaxation is no longer needed.

In summary, given the divergence-free initial velocity vector, the velocity vector $\underline{u}$ at the time step $(n+1)$ can be computed explicitly from Eq. (3.13). The source terms for M_3 and M_4 are computed respectively from Eqs. (3.16) and (3.15). As for the source term $-\nabla p'$, it is calculated from its central approximation (or $p'_{i,j}=\frac{p'_{i+1,j}-p'_{i-1,j}}{2\Delta x}$) based on the p'values computed from Eqs. (3.23) and (3.24). The pressure solution $p_{i,j}$ at $(n+1)\Delta t$ is then computed as $p^{n+1}_{i,j}=p^*_{i,j}+p'_{i,j}$, where p^* is the known convergent value calculated at the previous time (or $p^n_{i,j}$). The algorithm is summarized below:*Given the divergence-free initial velocity vector* $\underline{u}^*$ and p^* *with* $p'=0$

(1) $s := 0$;
(2) solving Eq. (3.13) to get the velocity vector $\underline{u}^{n+1}_s$ using Eqs. (3.16) and (3.15);
(3) solving Eqs. (3.23) and (3.24) to get p'_s;
(4) update p by virtue of $p^*_s = p^*_{s-1}+p'_s$;
(4) $s := s+1$;
(5) check convergence {if convergence, go to step (1) to compute the solution at the next time step; otherwise, go to step (2)}.

4. Discretization of spatial derivatives in non-staggered grids

4.1. Approximation of pressure gradient terms

While the even–odd pressure oscillations can be well resolved in staggered grids, the resulting programming complexity motivated us to discretize ∇p in non-staggered meshes, where the velocities and pressure are stored at the same point. To avoid spurious pressure oscillations, the nodal value of $p_{i,j}$ should be taken into account while approximating ∇p at a nodal point (i,j). One novel way to approximate p_x (or $F_{i,j}$ $(\equiv hp_x|_{i,j})$) at an interior node (i,j) is to use the following implicit equation

$$c_1F_{i+1,j}+c_2F_{i,j}+c_3F_{i-1,j} = c_4(p_{i+2,j}-p_{i+1,j})+c_5(p_{i+1,j}-p_{i,j})+c_6(p_{i,j}-p_{i-1,j}) + c_7(p_{i-1,j}-p_{i-2,j}). \tag{4.1}$$

In the above equation, h denotes the constant mesh size. The readers can refer to [6] for the detailed derivation of the seven coefficients c_1–c_7 by expanding $F_{i\pm1,j}$ in Taylor series with respect to $F_{i,j}$, and $p_{i\pm1,j}$ and $p_{i\pm2,j}$ with respect to $p_{i,j}$.

4.2. Approximation of convective terms

The first-order spatial derivative terms shown in the linearized momentum equations are approximated such that their dispersion relations, which stand for the relation between the angular frequency of the wave and the wavenumber of the first-order derivative term, are retained so that the convective oscillations can be effectively suppressed in the prevailing convection case [23]. For the sake of simplicity, we present the way of approximating ϕ_x, which can accommodate the dispersion-relation-preserving property, under $\Delta x=\Delta y=h$. Referring to Fig. 1, ϕ_x at the nodal point (i,j) is assumed to be expressed as

$$\phi_x(x,y) \simeq \frac{1}{h}(a_1\phi_{i-1,j-1}+a_2\phi_{i,j-1}+a_3\phi_{i+1,j-1} + a_4\phi_{i-1,j}+a_5\phi_{i,j}+a_6\phi_{i+1,j}+a_7\phi_{i-1,j+1} + a_8\phi_{i,j+1}+a_9\phi_{i+1,j+1}+a_{10}\phi_{i,j-2} + a_{11}\phi_{i,j+2}+a_{12}\phi_{i-2,j}). \tag{4.2}$$

Substitution of the Taylor series expansions for $\phi_{i\pm1,j}$, $\phi_{i-2,j}$, $\phi_{i,j\pm1}$, $\phi_{i,j\pm2}$, $\phi_{i\pm1,j\pm1}$ into the above equation, we are led to derive the resulting modified equation for ϕ_x. The derivation is followed by eliminating eleven leading error terms to yield a system of eleven algebraic equations. One more equation has to be derived so as to be able to uniquely determine $a_1\sim a_{12}$ shown in Eq. (4.2). It is essential that the dispersion relation, which stands for the relation between the angular frequency of the wave and the wavenumber of the spatial variable, be retained so as to effectively

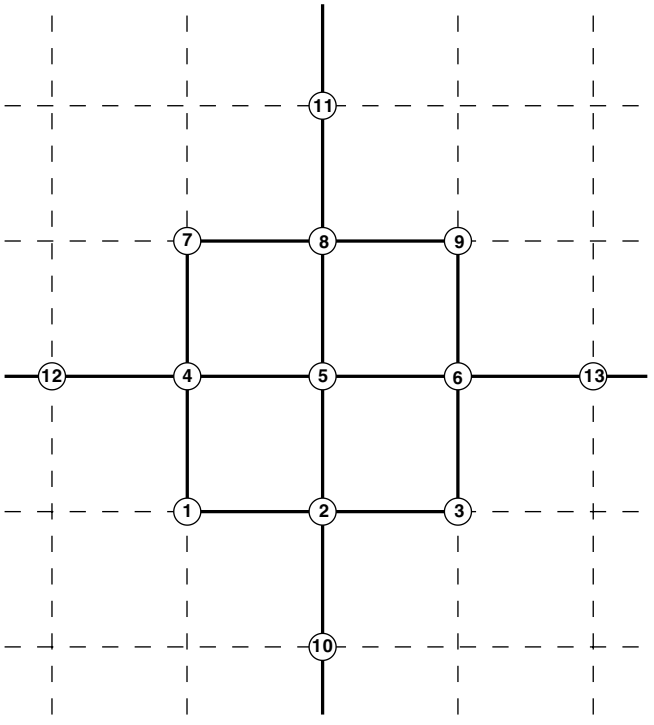

Fig. 1. Schematic of the stencil points invoked in the proposed two-dimensional DRP convection scheme.

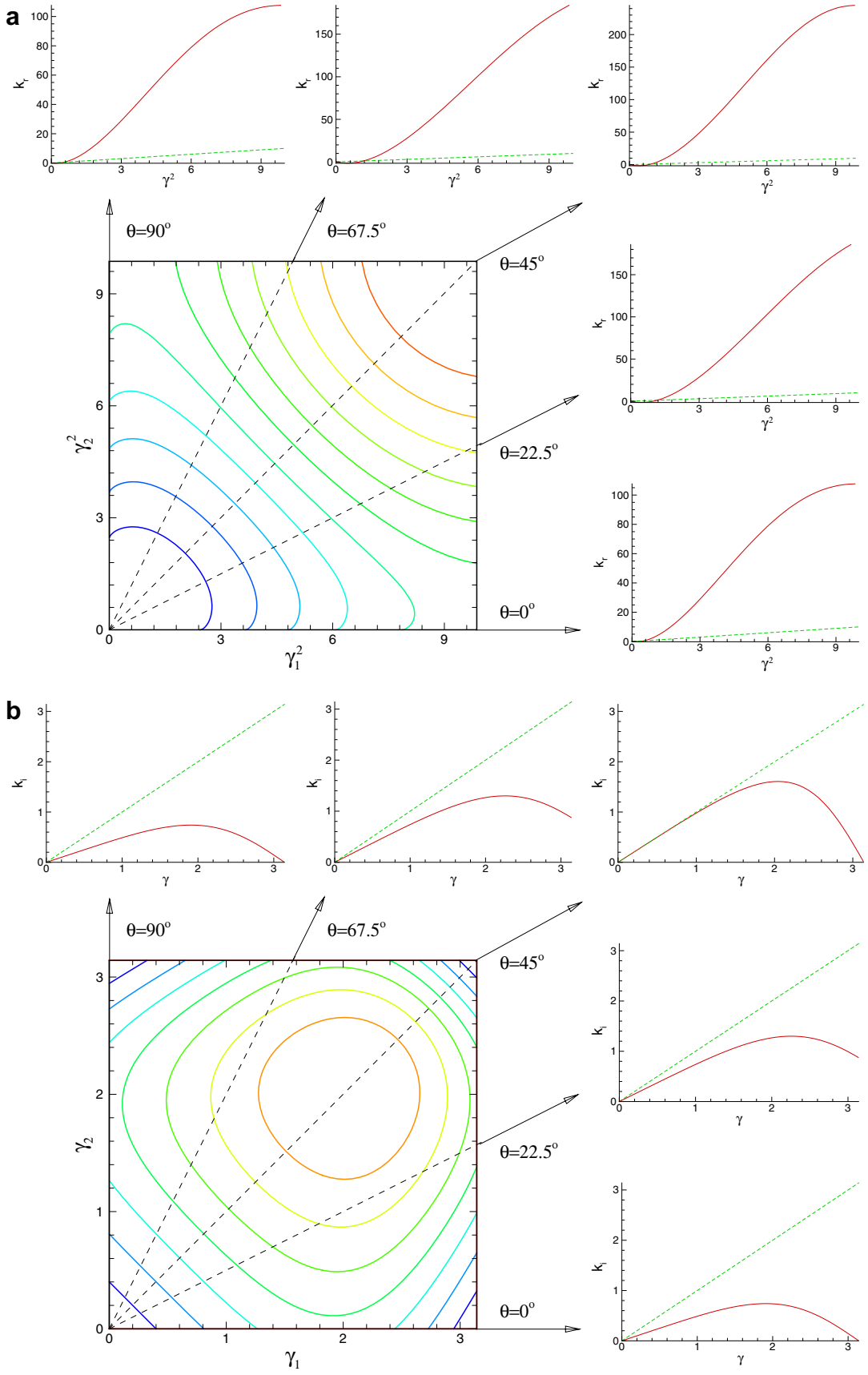

Fig. 2. Plots of k_r and k_i against (γ_1^2, γ_2^2) and (γ_1, γ_2), respectively, using the proposed scheme described in Section 4.2 for the cases investigated at $Pe_x = Pe_y = 10^2$, $R_x = R_y = 0$ and $v_x = v_y = 0.1$. (a) k_r; (b) k_i. Note that the dashed lines in the k_i–r and k_r–r^2 plots represent the exact solutions.

suppress the convective oscillations in the prevailing convection case [23]. The right-hand-side of Eq. (4.2) is desired to get nearly the same Fourier transform in space as the original derivative term shown in the left-hand-side of Eq. (4.2).

Within the two-dimensional context, defining the Fourier transform and its inverse for $\phi(x,y)$ as follows:

$$\tilde{\phi}(\alpha,\beta) = \frac{1}{(2\pi)^2}\int_{-\infty}^{+\infty}\int_{-\infty}^{+\infty}\phi(x,y)\mathrm{e}^{-\mathrm{i}(\alpha x+\beta y)}\,\mathrm{d}x\,\mathrm{d}y, \tag{4.3}$$

$$\phi(x,y) = \int_{-\infty}^{+\infty}\int_{-\infty}^{+\infty}\tilde{\phi}(\alpha,\beta)\mathrm{e}^{\mathrm{i}(\alpha x+\beta y)}\,\mathrm{d}\alpha\,\mathrm{d}\beta. \tag{4.4}$$

Performing the Fourier transform on terms shown in Eq. (4.2), the first component in the actual wavenumber vector $\underline{\alpha} = (\alpha,\beta)$ can be derived as

$$\begin{aligned}\alpha \simeq \frac{-\mathrm{i}}{h}(&a_1\mathrm{e}^{-\mathrm{i}(\alpha h+\beta h)} + a_2\mathrm{e}^{-\mathrm{i}\beta h} + a_3\mathrm{e}^{\mathrm{i}(\alpha h-\beta h)} + a_4\mathrm{e}^{-\mathrm{i}\alpha h}\\ &+ a_5 + a_6\mathrm{e}^{\mathrm{i}\alpha h} + a_7\mathrm{e}^{-\mathrm{i}(\alpha h-\beta h)} + a_8\mathrm{e}^{\mathrm{i}\beta h} + a_9\mathrm{e}^{\mathrm{i}(\alpha h+\beta h)}\\ &+ a_{10}\mathrm{e}^{\mathrm{i}(-2\beta h)} + a_{11}\mathrm{e}^{\mathrm{i}(2\beta h)} + a_{12}\mathrm{e}^{\mathrm{i}(-2\alpha h)}),\end{aligned} \tag{4.5}$$

where $\mathrm{i} = \sqrt{-1}$. In the approximated sense, the two components of the effective wavenumber vector $\underline{\tilde{\alpha}} = (\tilde{\alpha},\tilde{\beta})$ can be written as follows

$$\begin{aligned}\tilde{\alpha} = \frac{-\mathrm{i}}{h}(&a_1\mathrm{e}^{-\mathrm{i}(\alpha h+\beta h)} + a_2\mathrm{e}^{-\mathrm{i}\beta h} + a_3\mathrm{e}^{\mathrm{i}(\alpha h-\beta h)} + a_4\mathrm{e}^{-\mathrm{i}\alpha h}\\ &+ a_5 + a_6\mathrm{e}^{\mathrm{i}\alpha h} + a_7\mathrm{e}^{-\mathrm{i}(\alpha h-\beta h)} + a_8\mathrm{e}^{\mathrm{i}\beta h} + a_9\mathrm{e}^{\mathrm{i}(\alpha h+\beta h)}\\ &+ a_{10}\mathrm{e}^{\mathrm{i}(-2\beta h)} + a_{11}\mathrm{e}^{\mathrm{i}(2\beta h)} + a_{12}\mathrm{e}^{\mathrm{i}(-2\alpha h)}),\end{aligned} \tag{4.6}$$

$$\begin{aligned}\tilde{\beta} = \frac{-\mathrm{i}}{h}(&b_1\mathrm{e}^{-\mathrm{i}(\alpha h+\beta h)} + b_2\mathrm{e}^{-\mathrm{i}\beta h} + b_3\mathrm{e}^{\mathrm{i}(\alpha h-\beta h)} + b_4\mathrm{e}^{-\mathrm{i}\alpha h}\\ &+ b_5 + b_6\mathrm{e}^{\mathrm{i}\alpha h} + b_7\mathrm{e}^{-\mathrm{i}(\alpha h-\beta h)} + b_8\mathrm{e}^{\mathrm{i}\beta h} + b_9\mathrm{e}^{\mathrm{i}(\alpha h+\beta h)}\\ &+ b_{10}\mathrm{e}^{\mathrm{i}(-2\beta h)} + b_{11}\mathrm{e}^{\mathrm{i}(2\beta h)} + b_{12}\mathrm{e}^{\mathrm{i}(-2\alpha h)}).\end{aligned} \tag{4.7}$$

To make $\tilde{\alpha}$ as an appropriate representation of α, it is rational to make the value of $|\alpha h - \tilde{\alpha}h|^2$ (or the following integrated error E) to be equal to zero in the following weak sense [23–25]:

$$\begin{aligned}E(\alpha) &= \int_{-\frac{\pi}{2}}^{\frac{\pi}{2}}\int_{-\frac{\pi}{2}}^{\frac{\pi}{2}}|\alpha h - \tilde{\alpha}h|^2\,\mathrm{d}(\alpha h)\mathrm{d}(\beta h)\\ &= \int_{-\frac{\pi}{2}}^{\frac{\pi}{2}}\int_{-\frac{\pi}{2}}^{\frac{\pi}{2}}|\mathrm{i}\gamma_1 - \tilde{\gamma}_1|^2\,\mathrm{d}\gamma_1\,\mathrm{d}\gamma_2.\end{aligned} \tag{4.8}$$

Note that $(\gamma_1,\gamma_2)(\equiv(\alpha h,\beta h))$ should sufficiently define a period of sine (or cosine) wave. This explains why the integral range shown above is chosen as $-\frac{\pi}{2} \leqslant \gamma_1,\ \gamma_2 \leqslant \frac{\pi}{2}$. To minimize E, $\frac{\partial E}{\partial a_6} = 0$ is enforced to obtain $a_1 = a_3 = a_7 = a_9 = 0$, $a_2 = a_8 = \frac{1}{9}\frac{\pi(3\pi-10)}{(3\pi-8)}$, $a_4 = -1$, $a_6 = \frac{1}{3}$, $a_5 = \frac{1}{6}\frac{3\pi^2-19\pi+24}{(3\pi-8)}$, $a_{10} = a_{11} = -\frac{1}{36}\frac{\pi(3\pi-10)}{(3\pi-8)}$, and $a_{12} = \frac{1}{6}$. In the

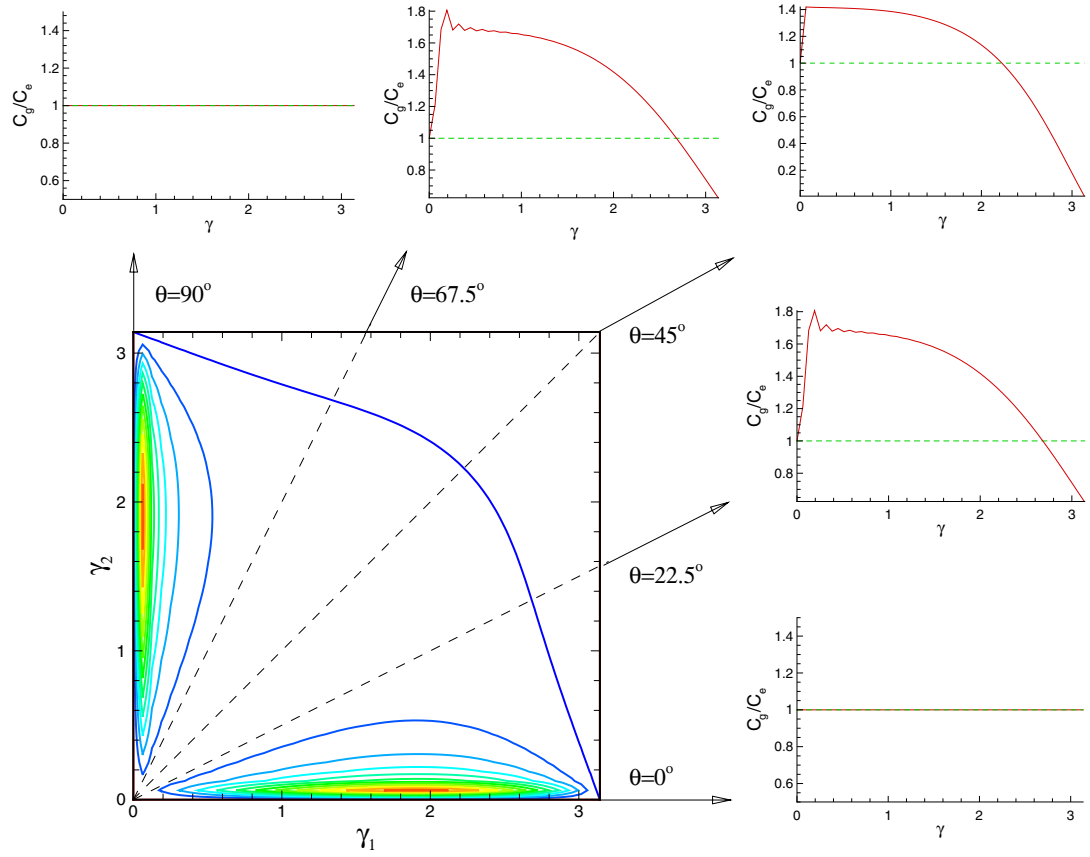

Fig. 3. Plots of the group velocity ratio $\frac{C_g}{C_e}$ against the modified wave-number (γ_1,γ_2) using the proposed scheme described in Section 4.2 for the cases investigated at $Pe_x = Pe_y = 10^2$, $R_x = R_y = 0$ and $v_x = v_y = 0.1$.

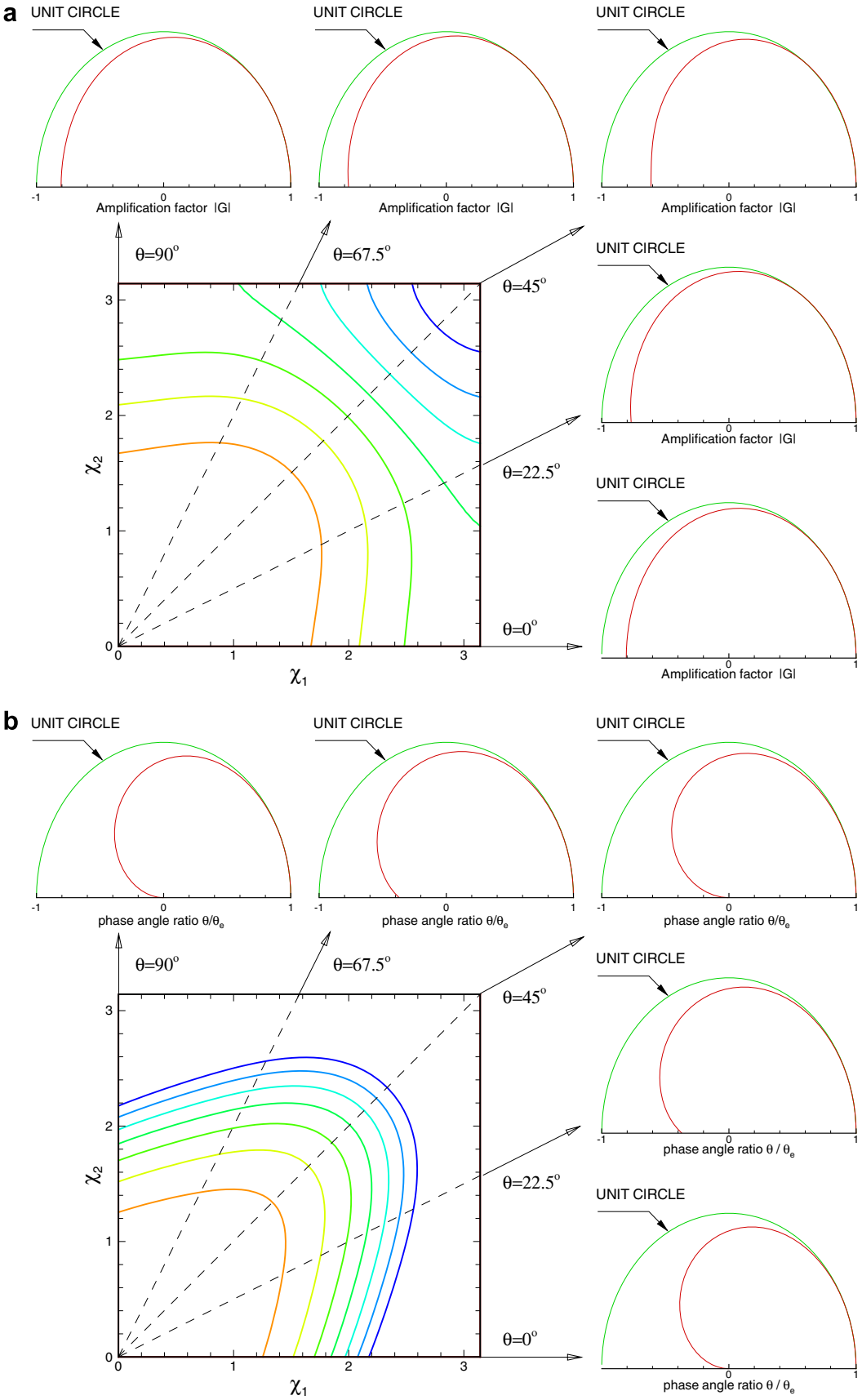

Fig. 4. Plots of the amplification factor $|G|$ and the phase angle ratio $\frac{\theta}{\theta_e}$ against (χ_1, χ_2) using the proposed scheme described in Section 4.2 for the cases investigated at $Pe_x = Pe_y = 10^2$, $R_x = R_y = 0$ and $v_x = v_y = 0.1$. (a) $|G|$; (b) $\frac{\theta}{\theta_e}$.

resulting modified equation, ϕ_x is shown to have a spatial accuracy order of three in the sense that $\phi_x \simeq \frac{h^3}{12}\phi_{xxxx} + \frac{h^3}{18}\frac{\pi(3\pi-10)}{(\pi^2-6\pi+8)}\phi_{yyyy} - \frac{h^4}{30}\phi_{xxxxx} + \frac{h^5}{72}\phi_{xxxxxx} + \cdots + \text{HOT}$. Similarly for ϕ_y, the 12-point stencil discrete equation, which accommodates the dispersion relation property, can be derived by the same way.

Dispersion and Fourier analyses will be conducted for the two-dimensional linear model equation given by $\frac{\phi^{n+1}-\phi^n}{\Delta t} + a\phi_x^n + b\phi_y^n - k\nabla^2\phi^n + c\phi^n = 0$. Given the initial condition $\phi(x,y,t=0) = \exp[\mathrm{i}(\alpha x + \beta y)]$, the exact solution for the two-dimensional Euler time-stepping scalar equation can be expressed in terms of (α,β)

$$\phi(x,y,t) = \exp\{-[k(\alpha^2+\beta^2)+c]t\}\exp\{\mathrm{i}[\alpha(x-at) + \beta(y-bt)]\}. \tag{4.9}$$

Referring to Fig. 1, the discrete equation at an interior point (i,j) takes the following form

$$\begin{aligned}\phi_{i,j}^{n+1} &= A_1\phi_{i-1,j-1}^n + A_2\phi_{i,j-1}^n + A_3\phi_{i+1,j-1}^n + A_4\phi_{i-1,j}^n \\ &+ A_5\phi_{i,j}^n + A_6\phi_{i+1,j}^n + A_7\phi_{i-1,j+1}^n + A_8\phi_{i,j+1}^n \\ &+ A_9\phi_{i+1,j+1}^n + A_{10}\phi_{i,j-2}^n + A_{11}\phi_{i,j+2}^n \\ &+ A_{12}\phi_{i-2,j}^n + A_{13}\phi_{i+2,j}^n.\end{aligned} \tag{4.10}$$

The exact solution for the above equation, which involves both amplitude and phase errors, is as follows

$$\begin{aligned}\tilde{\phi}(x,y,t) = \exp&\left\{-\left[\left(k\alpha^2+\frac{c}{2}\right)\frac{k_r}{\gamma_1^2} + \left(k\beta^2+\frac{c}{2}\right)\frac{k_r}{\gamma_2^2}\right]t\right\} \\ &\times \exp\left\{\mathrm{i}\left[\alpha\left(x - a\frac{k_i}{\gamma_1}t\right) + \beta\left(y - b\frac{k_i}{\gamma_2}t\right)\right]\right\}.\end{aligned} \tag{4.11}$$

By virtue of $(\gamma_1,\gamma_2) = (\alpha h, \beta h)$, $v_x = \frac{a\Delta t}{h}$, $v_y = \frac{b\Delta t}{h}$, $Pe_x = \frac{ah}{k}$, $Pe_y = \frac{bh}{k}$, $R_x = \frac{ch}{a}$ and $R_y = \frac{ch}{b}$, the following equation is derived

$$\begin{aligned}&\exp\left\{-\left\{\left[\left(k\alpha^2+\frac{c}{2}\right)\frac{k_r}{\gamma_1^2} + \left(k\beta^2+\frac{c}{2}\right)\frac{k_r}{\gamma_2^2}\right] + \mathrm{i}\left(\alpha a\frac{k_i}{\gamma_1} + \beta b\frac{k_i}{\gamma_2}\right)\right\}\Delta t\right\} \\ &= \exp\left\{-\left\{\left[\left(k\alpha^2+\frac{c}{2}\right)\frac{k_r}{(\alpha h)^2} + \left(k\beta^2+\frac{c}{2}\right)\frac{k_r}{(\beta h)^2}\right] \right.\right. \\ &\left.\left. + \mathrm{i}\left(\alpha a\frac{k_i}{\alpha h} + \beta b\frac{k_i}{\beta h}\right)\right\}\Delta t\right\}.\end{aligned} \tag{4.12}$$

Dispersion analysis of the semi-discrete equation is made by substituting $\phi_{i,j}$, $\phi_{i\pm1,j}$, $\phi_{i,j\pm1}$, $\phi_{i\pm2,j}$, $\phi_{i,j\pm2}$ and $\phi_{i\pm1,j\pm1}$, which are calculated from Eq. (4.11), into Eq. (4.10). By setting

$$\begin{aligned}&\exp\left\{-\left\{\left[\left(k\alpha^2+\frac{c}{2}\right)\frac{k_r}{\gamma_1^2} + \left(k\beta^2+\frac{c}{2}\right)\frac{k_r}{\gamma_2^2}\right]\right.\right. \\ &\left.\left. + \mathrm{i}\left(\alpha a\frac{k_i}{\gamma_1} + \beta b\frac{k_i}{\gamma_2}\right)\right\}\Delta t\right\} = \exp(\bar{p} + \mathrm{i}\bar{q}),\end{aligned}$$

the parameters accounting for the amplitude, k_r, and phase, k_i, errors can be derived as

$$k_r = \frac{-\bar{p}}{\frac{v_x}{Pe_x} + \frac{v_x}{Pe_x} + \frac{1}{2}\left(\frac{v_xR_x+1}{\gamma_1^2} + \frac{v_yR_y+1}{\gamma_2^2}\right)}, \tag{4.13}$$

$$k_i = \frac{-\bar{q}}{v_x + v_y}. \tag{4.14}$$

The exact expressions for $\phi_{i,j}$, $\phi_{i\pm1,j}$, $\phi_{i,j\pm1}$, $\phi_{i\pm2,j}$, $\phi_{i,j\pm2}$ and $\phi_{i\pm1,j\pm1}$, are then substituted into Eq. (4.10) to render the following expression

$$\begin{aligned}\mathrm{e}^{\bar{p}+\mathrm{i}\bar{q}} = (&A_1\mathrm{e}^{\mathrm{i}(-\bar{x})} + A_2\mathrm{e}^{\mathrm{i}(-\gamma_2)} + A_3\mathrm{e}^{\mathrm{i}(\bar{y})} + A_4\mathrm{e}^{\mathrm{i}(-\gamma_1)} \\ &+ A_5\mathrm{e}^{\mathrm{i}} + A_6\mathrm{e}^{\mathrm{i}(\gamma_1)} + A_7\mathrm{e}^{\mathrm{i}(-\bar{y})} + A_8\mathrm{e}^{\mathrm{i}(\gamma_2)} + A_9\mathrm{e}^{\mathrm{i}(\bar{x})} \\ &+ A_{10}\mathrm{e}^{\mathrm{i}(-2\gamma_2)} + A_{11}\mathrm{e}^{\mathrm{i}(2\gamma_2)} + A_{12}\mathrm{e}^{\mathrm{i}(-2\gamma_1)} + A_{13}\mathrm{e}^{\mathrm{i}(2\gamma_1)}),\end{aligned} \tag{4.15}$$

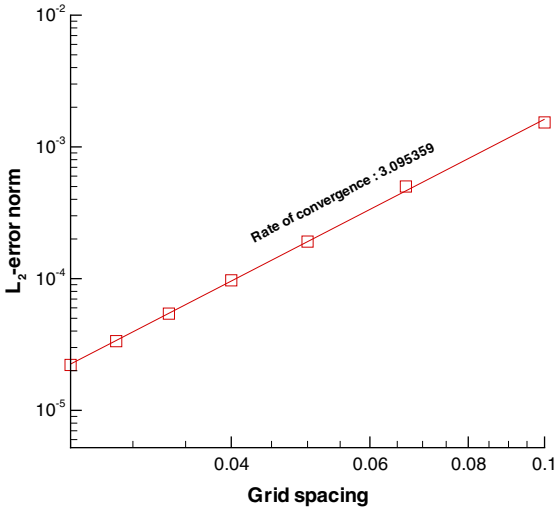

Fig. 5. The predicted spatial rate of convergence based on the L_2-error norms computed at $t = 1$ for the validation problem given in Section 5.1.

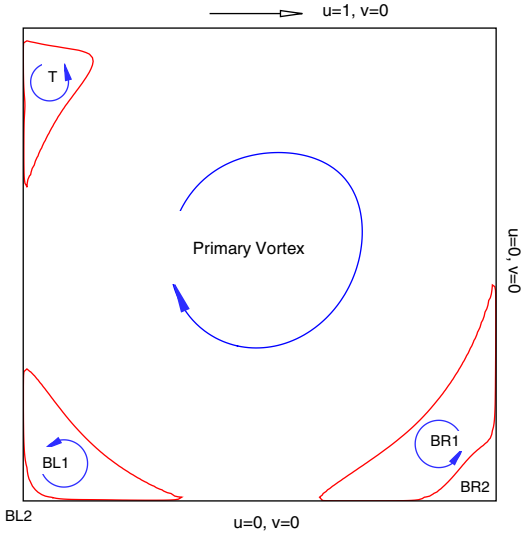

Fig. 6. Schematic of the simulated eddy centers in the lid-driven cavity.

where $\bar{x} = \gamma_1 + \gamma_2$ and $\bar{y} = \gamma_1 - \gamma_2$. Two variables $\bar{q}$ and $\bar{p}$ shown above can be derived as $\bar{q} = \tan^{-1}\frac{n}{m}$ and $\bar{p} = \ln\{m\cos\bar{q} + n\sin\bar{q}\}$ from the respective imaginary and real parts, where m and n are given below

$$m = (A_1 + A_9)\cos\bar{x} + (A_2 + A_8)\cos\gamma_2 + (A_3 + A_7)\cos\bar{y} + (A_4 + A_6)\cos\gamma_1 + A_5 + (A_{10} + A_{11})\cos(2\gamma_2) + (A_{12} + A_{13})\cos(2\gamma_1), \quad (4.16)$$

$$n = -[(A_1 - A_9)\sin\bar{x} + (A_2 - A_8)\sin\gamma_2 + (A_7 - A_3)\sin\bar{y} + (A_4 - A_6)\sin\gamma_1 + (A_{10} - A_{11})\sin(2\gamma_2) + (A_{12} - A_{13})\sin(2\gamma_1)]. \quad (4.17)$$

Fig. 2 plots the k_r and k_i contours against (v_x, v_y) and (Pe_x, Pe_y) at the condition of $(R_x, R_y) = (0, 0)$, for example. It can be observed from this figure that k_i agrees perfectly with (γ_1, γ_2) in the small wavenumber range. The larger the wavenumbers, the less satisfactory are the predicted phase and the amplitude errors. The ratio $\frac{C_g}{C_e}$ for the numerical group velocity $C_g\left(\equiv \frac{1}{2}\left(\frac{\mathrm{d}\omega}{\mathrm{d}\gamma_1} + \frac{d\omega}{d\gamma_2}\right)\right.$, where $\left.\omega \equiv \left(\alpha a\frac{k_i}{\gamma_1} + \beta b\frac{k_i}{\gamma_2}\right)\right)$, and the analytical wave velocity C_e is plotted in Fig. 3.

Fourier (or von Neumann) stability analysis [27] is also conducted. Let $\chi_x = \chi_y = \frac{2\pi m}{2L}h$ $(m = 0, 1, 2, 3, \ldots, M)$, h be the grid size, and $2L$ be the period of fundamental frequency $(m = 1)$, the amplification factor $G\left(\equiv \frac{\phi^{n+1}_{i,j}}{\phi^{n}_{i,j}}\right)$ can be derived as $G = \mathrm{e}^{\bar{p}}(\cos\bar{q} + \mathrm{i}\sin\bar{q})$. In Fig. 4a, $|G|$ is clearly seen to have a magnitude smaller than one at the low values of v_x and v_y. Take the case of $pe_x = pe_y = 10^2$ as an example, when $v_x = v_y \leqslant 0.25$ the value of $|G|$ is smaller than one. The derived amplification factor is rewritten as $G = |G|\mathrm{e}^{\mathrm{i}\theta}$, where $\theta\left(\equiv \tan^{-1}\left|\frac{\mathrm{Im}(G)}{\mathrm{Re}(G)}\right|\right)$ is the phase angle. According to the exact phase angle $\theta_e = -(\chi_x v_x + \chi_y v_y)$, the contour values for the relative phase shift $\frac{\theta}{\theta_e}$ are plotted against (χ_x, χ_y), (v_x, v_y) and (Pe_x, Pe_y) in Fig. 4b at the fixed value of $(R_x, R_y) = (0, 0)$.

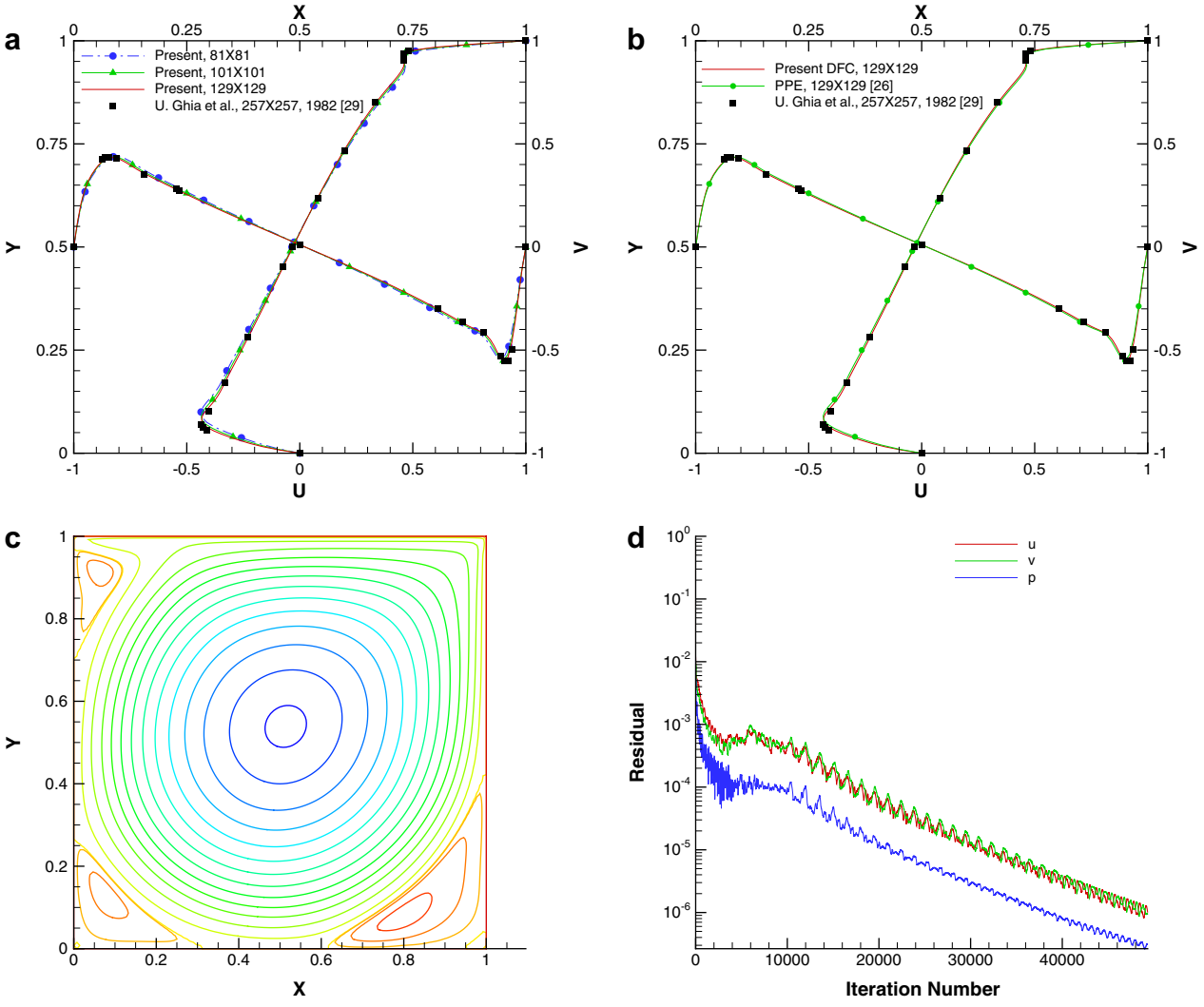

Fig. 7. Comparison of the simulated and Ghia's results obtained at $Re = 5000$. (a) velocity profiles $u(x, 0.5)$ and $v(0.5, y)$ obtained at different mesh sizes; (b) comparison of the simulated velocity profiles using the conventional PPE and the proposed DFC compensated methods; (c) the simulated streamfunction contours; (d) the simulated error reduction plots.

5. Numerical studies

5.1. Validation study

We consider the following transport equation for ϕ in a square domain $(-1 \leqslant x, y \leqslant 1)$ for the sake of code validation:

$$\frac{\partial \phi}{\partial t} + u\frac{\partial \phi}{\partial x} + v\frac{\partial \phi}{\partial y} = \frac{1}{Re}\left(\frac{\partial^2 \phi}{\partial x^2} + \frac{\partial^2 \phi}{\partial y^2}\right) + S. \tag{5.1}$$

In the above, Re and S denote the Reynolds number and the source per unit volume, respectively. The solution ϕ is sought in a domain subject to the following divergence-free velocity field [28]:

$$u(x, y, t) = -\cos(\pi x)\sin(\pi y)e^{-2\pi^2 t/Re}, \tag{5.2}$$

$$v(x, y, t) = \sin(\pi x)\cos(\pi y)e^{-2\pi^2 t/Re}. \tag{5.3}$$

The analytic solution for ϕ has the same form as u given in (5.2) provided that $S = -\frac{\partial p}{\partial x}$, where

$$p(x, y, t) = -\frac{1}{4}(\cos(2\pi x) + \cos(2\pi y))e^{-4\pi^2 t/Re}. \tag{5.4}$$

As usual, the employed DRP upwind discretization scheme is assessed by examining the predicted nodal errors obtained at various mesh sizes for $Re = 10^3$ and $\Delta t = 10^{-4}$. The rate of convergence is slightly larger than 3, as shown in Fig. 5, based on the L_2-error norms computed at different grid sizes of $h = \frac{1}{10}, \frac{1}{15}, \frac{1}{20}, \frac{1}{25}, \frac{1}{30}, \frac{1}{35}, \frac{1}{40}$. The applicability of the DRP scheme to solve the two-dimensional transport equation is, therefore, confirmed.

5.2. Lid-driven cavity flow problem

Fluid flow is analyzed at $Re = 5000$ in the lid-driven square cavity. For the cases with 81×81, 101×101 and 129×129 mesh points, the predicted velocity profiles $u(0.5, y)$ and $v(x, 0.5)$ plotted in Fig. 7 show good agreement with the steady-state benchmark solutions of Ghia [29]. Besides the good agreement with the benchmark locations of eddy centers, which are schematic in Fig. 6 and tabulated in Table 1, the considerable saving of CPU time shown in Fig. 8 demonstrates the benefit of applying the present scheme to carry out the high Reynolds number flow calculations. For the sake of completeness, the ratios of the CPU times required in the conventional PPE and the proposed DFC compensated approaches are also given in the same figure for the three additional cases investigated at $Re = 400$, 1000 and 3200. Based on the simulated results, we can estimate β, shown in Eq. (3.1) for the artificial compressibility method, and plot its magnitude against the iterations. It can be clearly seen from Fig. 9 that β is not the normally suggested constant value [17,18]. Instead, it is

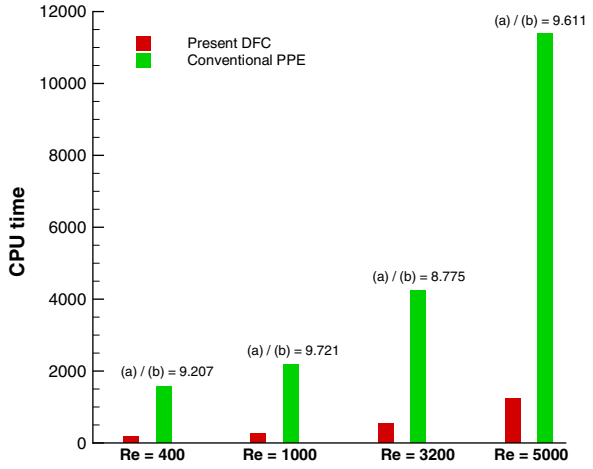

Fig. 8. Comparison of the CPU times, marked by (a), using the conventional PPE method and the CPU time, marked by (b), using the proposed DFC compensated method.

Table 1
Comparison of the predicted eddy centers (primary eddy P, corner eddies BL and BR, and the eddy T near the cavity roof schematic in Fig. 6) with those reported in [26,29] for the lid-driven cavity problem investigated at $Re = 400$, 1000, 3200 and 5000

Symbol	Authors	R			
		400	1000	3200	5000
Primary	PPE [26]	0.5599, 0.6062	0.5332, 0.5658	0.5180, 0.5453	0.5138, 0.5356
	Ghia [29]	0.5547, 0.6055	0.5313, 0.5625	0.5165, 0.5469	0.5117, 0.5352
	Present DFC	0.5570, 0.6068	0.5311, 0.5637	0.5173, 0.5464	0.5138, 0.5378
T	PPE [26]	–	–	0.0532, 0.8965	0.0643, 0.9149
	Ghia [29]	–	–	0.0547, 0.8984	0.0625, 0.9141
	Present DFC	–	–	0.0546, 0.9025	0.0632, 0.9154
BL	PPE [26]	0.0495, 0.0468	0.0846, 0.0787	0.0838, 0.1102	0.0730, 0.1337
	Ghia [29]	0.0508, 0.0469	0.0859, 0.0781	0.0859, 0.1094	0.0703, 0.1367
	Present DFC	0.0505, 0.0463	0.0850, 0.0776	0.0827, 0.1148	0.0738, 0.1337
BR	PPE [26]	0.8859, 0.1235	0.8640, 0.1098	0.8203, 0.0876	0.8000, 0.0760
	Ghia [29]	0.8906, 0.1250	0.8594, 0.1094	0.8125, 0.0859	0.8086, 0.0742
	Present DFC	0.8861, 0.1251	0.8626, 0.1105	0.8194, 0.0868	0.8000, 0.0762
Mesh points	PPE [26]	101	129	129	129
	Ghia [29]	257	129	129	257
	Present DFC	101	129	129	129

varied dramatically in the course of calculations. The proposed method is also applied to solve the two-dimensional transient lid-driven cavity problem. For the cases investigated at $Re = 400$, 101×101 mesh points and $\Delta t = 10^{-3}$, the predicted velocity profiles $u(0.5, 0.8)$ and $u(0.5, 0.2)$ in Fig. 10 show good agreement with the predicted solutions of Pontaza [30].

For the sake of completeness, the proposed method is also applied to solve the three-dimensional lid-driven cavity problem in a square cube at $Re = 400$ and 1000. Comparison was made on the basis of the predicted mid-span velocity profiles along the vertical and horizontal centerlines. According to the computed solutions plotted in Fig. 11, the agreement with the solutions given in [31–33] is known to be excellent.

5.3. Natural convection problem

Two-dimensional natural convection problem for the unit square cavity ($0 \leqslant x, y \leqslant 1$) schematic in Fig. 12 is governed by the following equations:

$$\frac{\partial u}{\partial x} + \frac{\partial v}{\partial y} = 0, \tag{5.5}$$

$$\frac{\partial u}{\partial t} + u\frac{\partial u}{\partial x} + v\frac{\partial u}{\partial y} = -\frac{\partial p}{\partial x} + Pr\left(\frac{\partial^2 u}{\partial x^2} + \frac{\partial^2 u}{\partial y^2}\right), \tag{5.6}$$

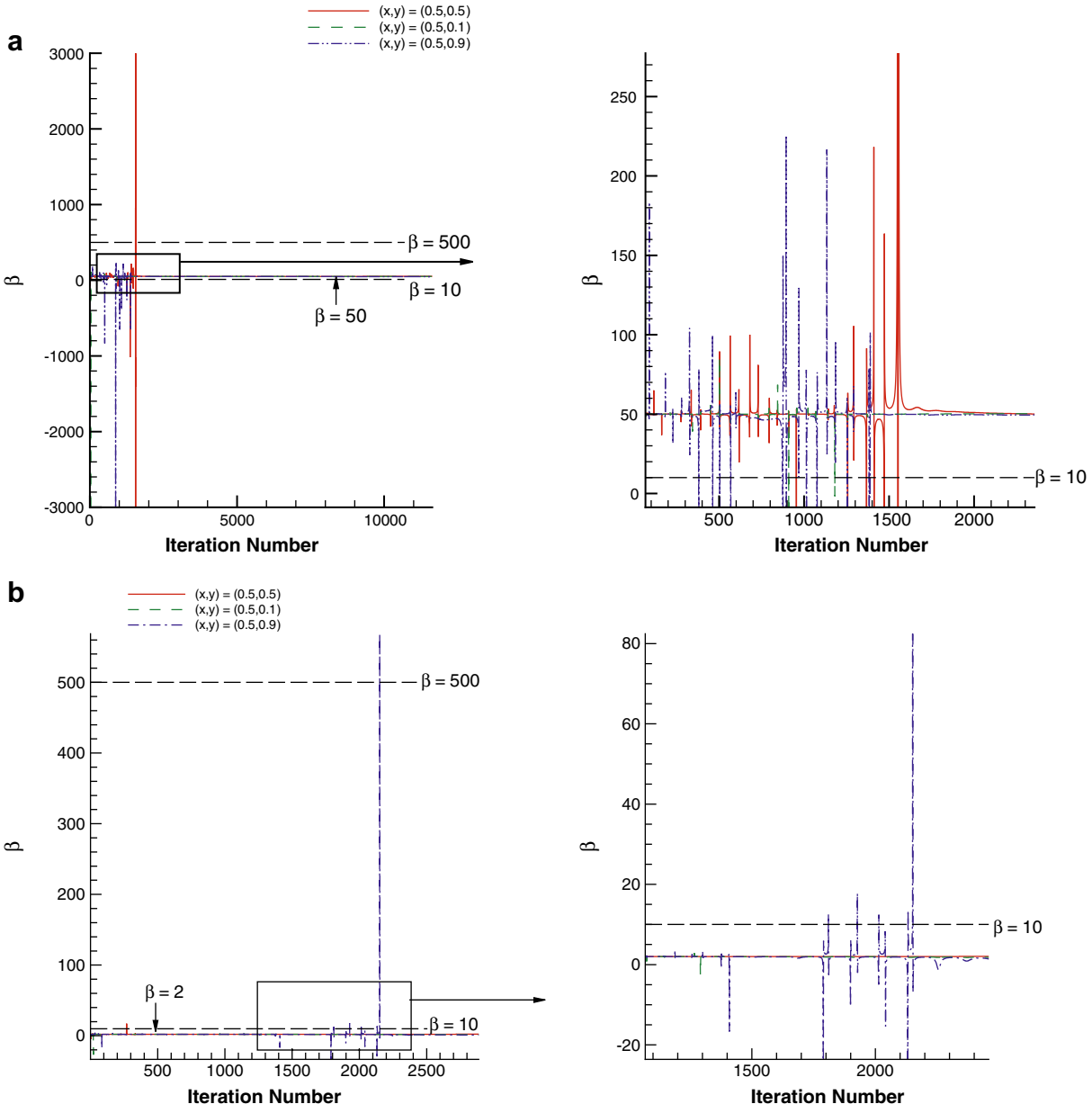

Fig. 9. Plots of the magnitude of $\beta(\equiv -\frac{\Delta p}{\nabla \cdot u \Delta t})$ based on the simulated solutions for the lid-driven cavity problem investigated at $Re = 400$ using the present DFC compensated method with 41×41 grids. (a) CFL = 0.1; (b) CFL = 0.5. Note that β in the range of $10 \leqslant \beta \leqslant 500$ was recommended in [17,18].

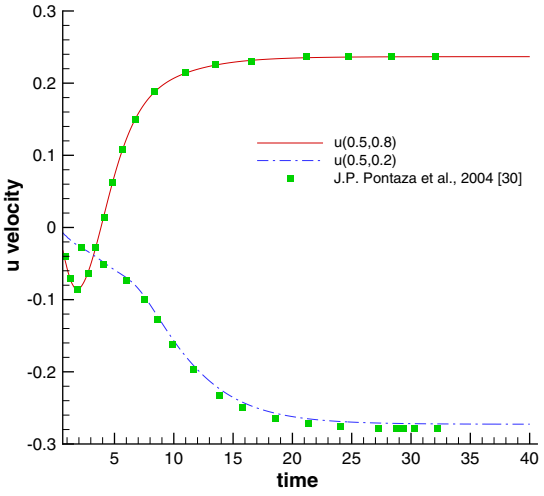

Fig. 10. Comparison of the simulated and Pontaza's results investigated at $Re = 400$ for the velocity profiles $u(0.5, 0.8)$ and $u(0.5, 0.2)$ obtained at 101×101 meshes and $\Delta t = 10^{-3}$.

$$\frac{\partial v}{\partial t} + u\frac{\partial v}{\partial x} + v\frac{\partial v}{\partial y} = -\frac{\partial p}{\partial y} + Pr\left(\frac{\partial^2 v}{\partial x^2} + \frac{\partial^2 v}{\partial y^2}\right) + RaPrT, \quad (5.7)$$

$$\frac{\partial T}{\partial t} + u\frac{\partial T}{\partial x} + v\frac{\partial T}{\partial y} = \frac{\partial^2 T}{\partial x^2} + \frac{\partial^2 T}{\partial y^2}. \quad (5.8)$$

The boundary conditions for velocity at all walls are no-slip ($u = v = 0$), while the temperatures along the two vertical walls are $T = 1$ at $x = 0$ and $T = 0$ at $x = 1$. Along the horizontal walls, both of them are assumed to be adiabatic $\left(\frac{\partial T}{\partial y} = 0\right)$. The problem is investigated at Ra(Rayleigh number) $= 10^3, 10^4, 10^5, 10^6, 10^7$ and Pr (Prandtl number)$= 0.71$. In the current study, uniform mesh of nodal points 81×81 is employed for the cases investigated at $Ra = 10^3, 10^4$ and 129×129 nodal points for the cases with $Ra = 10^5, 10^6, 10^7$. The solutions plotted in Fig. 13 and tabulated in Tables 2–4 are compared well with the referenced

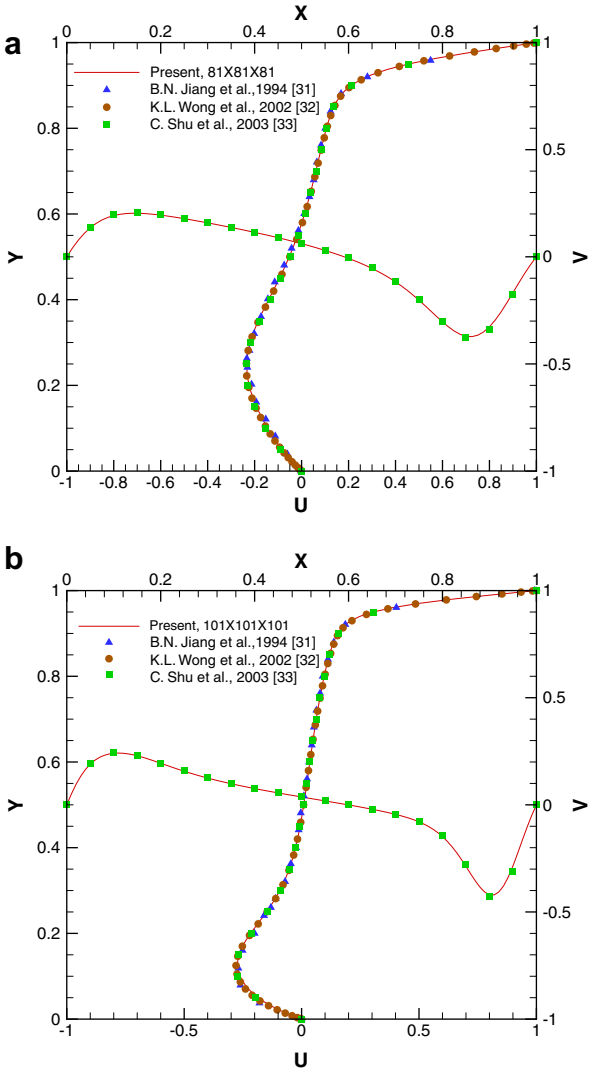

Fig. 11. Comparison of the predicted three-dimensional lid-driven cavity velocity profiles $u(x, 0.5, 0.5)$ and $v(0.5, y, 0.5)$. (a) $Re = 400$; (b) $Re = 1000$.

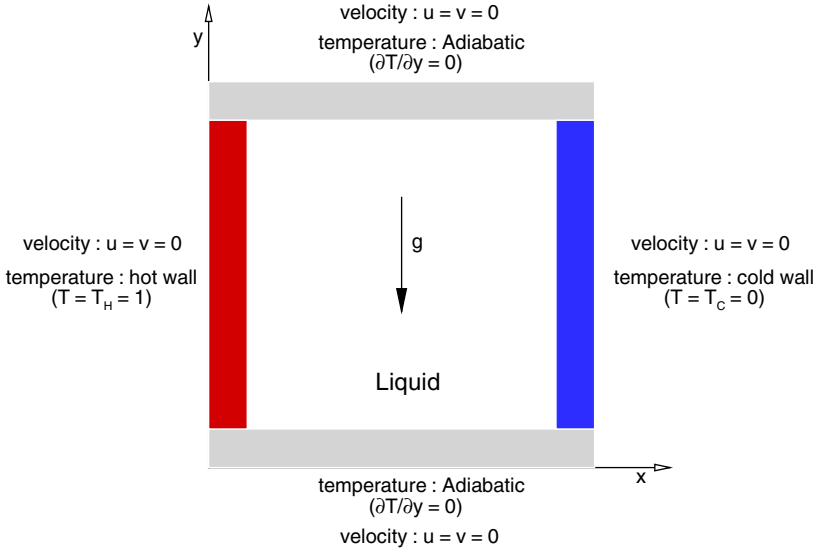

Fig. 12. Schematic of the natural convection problem.

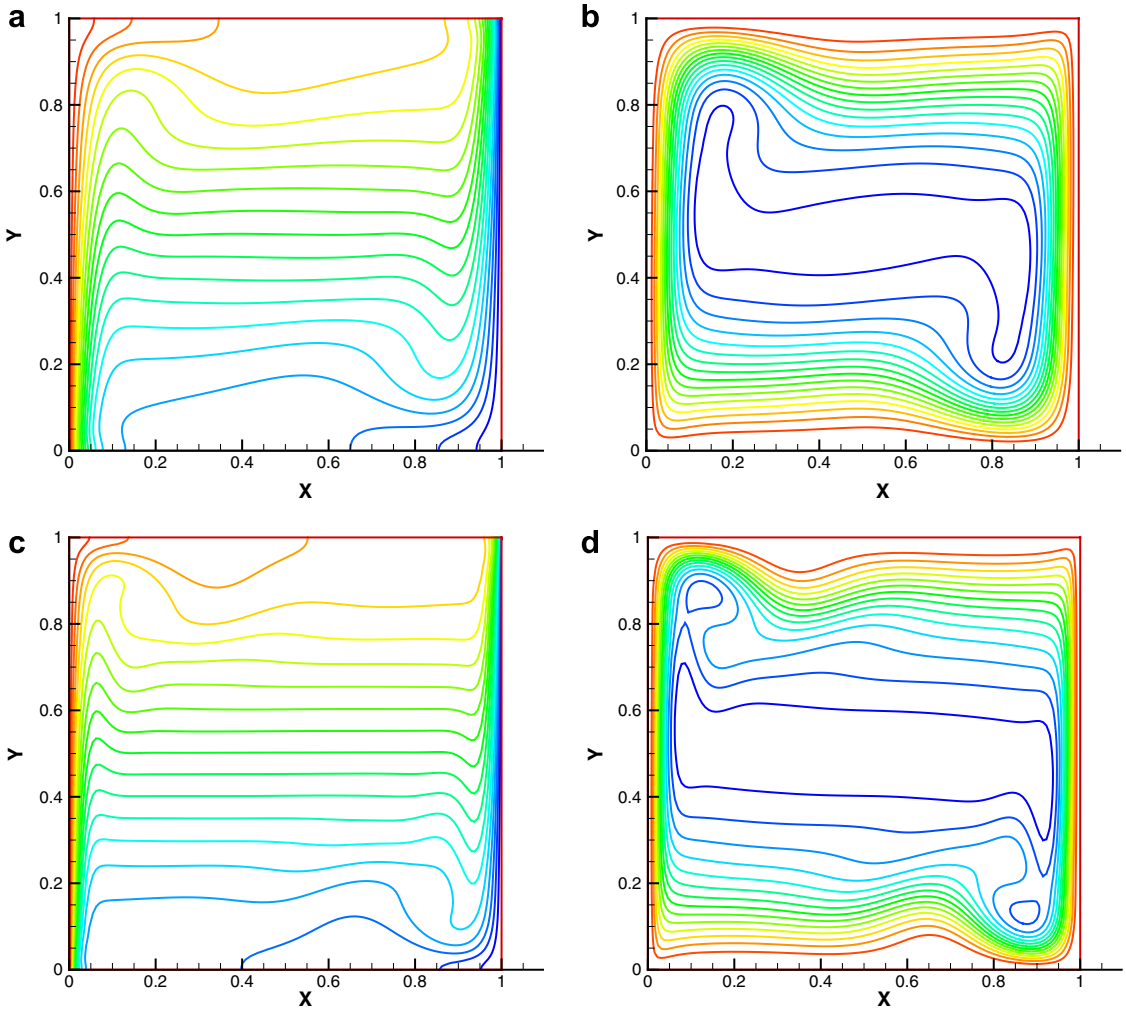

Fig. 13. The simulated temperature and streamfunction contours for the natural convection problem. (a) and (b) $Ra = 10^6$; (c) and (d) $Ra = 10^7$.

Table 2
Comparison of the predicted values for the streamfunction at (0.5, 0.5) with other solutions reported in [26,34]

Ra	10^3	10^4	10^5	10^6	10^7
De Vahl Davis [34]	1.174	5.071	9.111	16.32	–
Ramaswamy, Jue and Akin [34]	1.170	5.099	9.217	16.68	29.436
Le Quéré [34]	–	–	–	16.38	29.362
Dennis and Hudson [34]	1.175	5.074	9.113	–	–
Kalita, Dalal and Dass [34]	1.175	5.080	9.123	16.42	29.382
Conventional PPE [26]	1.175	5.071	9.113	16.42	29.432
Present work	1.174	5.070	9.103	16.35	29.380

Table 3
Comparison of the predicted maximum velocity magnitudes for v at $(0.5, y)$ with those reported in [26,34]

Ra	10^3	10^4	10^5	10^6	10^7
Chenoweth and Paolucci [34]	3.695	19.62	68.63	220.8	699.0
De Vahl Davis [34]	3.697	19.62	68.63	219.4	–
Ramaswamy, Jue and Akin [34]	–	19.62	68.64	232.97	717.04
Le Quéré [34]	–	–	–	220.56	699.2
Saitoh and Hirosh [34]	–	19.62	–	216.76	–
Ho and Lin [34]	3.697	19.63	68.63	219.86	705.3
Hortmann, Peric and Scheure [34]	–	19.63	68.64	220.46	–
Dennis and Hudson [34]	3.698	19.63	68.64	–	–
Kalita, Dalal and Dass [34]	3.697	19.61	68.61	221.66	696.2
Conventional PPE [26]	3.695	19.61	68.55	219.88	695.6
Present work	3.695	19.54	68.50	219.16	692.3

Table 4
Comparison of the simulated averaged Nusselt numbers $\overline{Nu}$ with those reported in [26,34]

Ra	10^3	10^4	10^5	10^6	10^7
Chenoweth and Paolucci [34]	1.118	2.244	4.520	8.822	16.82
De Vahl Davis [34]	1.118	2.243	4.519	8.800	–
Le Quéré [34]	–	–	–	8.825	16.52
Hortmann, Peric and Scheure [34]	–	2.245	4.521	8.825	–
Saitoh and Hirosh [34]	–	2.242	–	8.712	–
Ball and Kuo [34]	1.118	2.248	4.528	8.824	16.52
Ho and Lin [34]	1.118	2.248	4.528	8.824	16.52
Comini, Cortella and Manzan [34]	–	–	4.503	8.825	16.53
Kalita, Dalal and Dass [34]	1.118	2.245	4.522	8.829	16.52
Conventional PPE [26]	1.118	2.242	4.528	8.822	16.80
Present work	1.118	2.241	4.515	8.820	16.70

Table 5
Comparison of the CPU times, marked by (a), required for the conventional PPE method and the CPU time, marked by (b), using the present compensated method

Ra	10^3	10^4	10^5	10^6	10^7
Conventional PPE [26]	6975.32	7936.64	–	–	–
Present work	669.59	745.95	3145.79	4314.01	12307.45
(a)/(b)	10.417	10.639			

Note that "–" indicates the cases having the CPU time $\geqslant 20000$.

numerical solutions. As the computed results tabulated in Table 5, the saving of CPU time is seen to be considerable.

6. Concluding remarks

In the current study, the divergence-free-condition compensated method is proposed to solve the two-dimensional incompressible viscous equations. The simulated results from the dispersion-relation-preserving convection scheme for the first-order derivatives in non-staggered grids demonstrate that the simulated solutions have good agreement with the benchmark solutions for the lid-driven cavity and natural convection problems. A considerable amount of the computational time is also seen to be reduced.

Acknowledgements

This work was supported by the National Science Council of the Republic of China under Grants NSC-94-2611-E-002-021 and NSC-94-2745-P-002-002.

References

[1] J.E. Fromm, F.H. Harlow, Numerical solution of the problem of vortex street development, Phys. Fluids 6 (1963) 975–982.
[2] F.H. Harlow, J.E. Welch, Numerical calculation of time dependent viscous incompressible flow of fluid with free surface, Phys. Fluids 8 (1965) 2182–2188.
[3] S.V. Patankar, A calculation procedure for two-dimensional elliptic situations, Numer. Heat Transfer 4 (1981) 409–425.
[4] S.V. Patankar, Numerical Heat Transfer and Fluid Flow, Hemisphere, New York, 1980.
[5] J. Papageorgakopoulos, G. Arampatzis, D. Assimacopoulos, N.C. Markatos, Enhancement of the momentum interpolation method on non-staggered grids, Int. J. Numer. Methods Fluids 33 (2000) 1–12.
[6] Tony W.H. Sheu, R.K. Lin, An incompressible Navier–Stokes model implemented on non-staggered grids, Numer. Heat Transfer B, Fundam. 44 (2003) 277–294.
[7] F. Brezzi, M. Fortin, Mixed and Hybrid Finite Element Methods, Springer-Verlag, New York, 1991.
[8] A.J. Chorin, Numerical solution of the Navier–Stokes equations, Math. Comput. 22 (1968) 745–762.
[9] R. Temam, Navier–Stokes Equations – Theory and Numerical Analysis, Elsevier, New York, 1984.
[10] V. Girault, P.A. Raviart, Finite Element Methods for Navier–Stokes Equations – Theory and Algorithms, Springer-Verlag, Berlin, 1986.
[11] E. Weinan, J.G. Liu, Gauge method for viscous incompressible flows, Commun. Math. Sci. 1 (2003) 317–332.
[12] E. Bayo, A. Avello, Singularity-free augmented Lagrangian algorithms for constrained multibody dynamics, Nonlinear Dyn. 5 (1994) 209–231.
[13] M. Fortin, R. Glowinski, Augmented Lagrangian Methods: Applications to the Numerical Solution of Boundary-Value Problems, North Holland, Amsterdam, 1983.
[14] P. Lin, A sequential regularization method for time-dependent incompressible Navier–Stokes equations, SIAM J. Numer. Anal. 34 (1997) 1051–1071.
[15] Morten M.T. Wang, Tony W.H. Sheu, An element-by-element BICGSTAB iterative method for three-dimensional steady Navier–Stokes equations, J. Comput. Appl. Math. 79 (1997) 147–165.
[16] L. Quartapelle, M. Napolitano, Integral conditions for the pressure in the computation of incompressible viscous flows, J. Comput. Phys. 62 (1986) 340–348.
[17] S.E. Rogers, D. Kwak, Upwind differencing scheme for the time-accurate incompressible Navier–Stokes equations, AIAA J. 28 (1990) 253–262.
[18] S.E. Rogers, D. Kwak, C. Kiris, Steady and unsteady solutions of the incompressible Navier–Stokes equations, AIAA J. 29 (1991) 603–610.
[19] O.A. Ladyzhenskaya, The Mathematical Theory of Viscous Incompressible Flow, Gordon and Breach, New York, 1969.
[20] G.I. Marchuk, Methods of Numerical Mathematics, Springer, New York, 1975.
[21] R. Temam, Remark on the pressure boundary condition for the projection method, Theor. Comput. Fluid Dyn. 3 (1991) 181–184.
[22] S.A. Orszag, M. Israeli, M.O. Deville, Boundary conditions for incompressible flows, J. Sci. Comput. 1 (1986) 75–111.
[23] C. Bogry, C. Bailly, A family of low dispersive and low dissipative explicit schemes for flow and noise computations, J. Comput. Phys. 194 (2004) 194–214.
[24] C.K.W. Tam, J.C. Webb, Dispersion-relation-preserving finite difference schemes for computational acoustics, J. Comput. Phys. 107 (1993) 262–281.

[25] I.A. Abalakin, A.V. Alexandrov, V.G. Bobkov, T.K. Kozubskaya, High accuracy methods and software development in computational aeroacoustics, J. Comput. Methods Sci. Engrg. 2 (2003) 1–14.
[26] P.H. Chiu, Tony W.H. Sheu, R.K. Lin, Development of a dispersion-relation-preserving upwinding scheme for incompressible Navier–Stokes equations on non-staggered grids, Numer. Heat Transfer B, Fundam. 48 (2005) 543–569.
[27] J. von Neumann, R.D. Richtmyer, A method for the numerical calculation on hydrodynamic shock, J. Appl. Phys. 21 (1950) 232–237.
[28] J. Kim, P. Moin, Application of a fractional step method to incompressible Navier–Stokes equations, J. Comput. Phys. 59 (1985) 308–323.
[29] U. Ghia, K.N. Ghia, C.T. Shin, High-Re solutions for incompressible flow using the Navier–Stokes equations and a multigrid method, J. Comput. Phys. 48 (1982) 387–411.
[30] J.P. Pontaza, J.N. Reddy, Space-time coupled spectral/hp least-squares finite element formulation for the incompressible Navier–Stokes equations, J. Comput. Phys. 197 (2004) 418–459.
[31] B.N. Jiang, T.L. Lin, L.A. Povinelli, Large-scale computation of incompressible viscous flow by least-squares finite element method, Comput. Methods Appl. Mech. Engrg. 114 (1994) 213–231.
[32] K.L. Wong, A.J. Baker, Numerical computation of three-dimensional incompressible Navier–Stokes equations in primitive variable form by DQ method, Int. J. Numer. Methods Fluids 38 (2002) 99–123.
[33] C. Shu, L. Wang, Y.T. Chew, Numerical computation of three-dimensional incompressible Navier–Stokes equations in primitive variable form by DQ method, Int. J. Numer. Methods Fluids 43 (2003) 345–368.
[34] J.C. Kalita, D.C. Dalal, A.K. Dass, Fully compact higher-order computation of steady-state natural convection in a square cavity, Phys. Rev. E 64 (2001) 066703.